Automatic Detection and Segmentation of Evolving Processes in 3D Medical Images: Application to Multiple Sclerosis

David Rey, Gérard Subsol, Hervé Delingette, and Nicholas Ayache

INRIA Sophia Antipolis, EPIDAURE project, France
David.Rey@sophia.inria.fr

Abstract. Physicians often perform diagnoses based on the evolution of lesions, tumors or anatomical structures through time. The objective of this paper is to automatically detect regions with apparent local volume variation with a vector field operator applied to the local displacement field obtained after a non-rigid registration between successive temporal images. In studying the information of apparent shrinking areas in the direct and reverse displacement fields between images, we are able to segment evolving lesions. Then we propose a method to segment lesions in a whole temporal series of images. In this paper we apply this approach to the automatic detection and segmentation of multiple sclerosis lesions in time series of MRI images of the brain.

1 Introduction

1.1 Multiple Sclerosis Data

Multiple sclerosis is a progressive disease that requires an evolution study through time. The evolution of the disease can be followed on a patient with a temporal series of examinations. A time series of 3D images of a patient is acquired from the same modality and with a definite protocol to have similar properties: similar histogram, field of view, voxel size, image size, etc. In this paper we use two sets of multiple sclerosis time series composed of T2 weighted MRI images. These two time series come from the Brigham and Women's Hospital [1] and from the BIOMORPH [2] European project. The data from the Brigham and Women's Hospital consist in $256 \times 256 \times 54$ images, with a voxel size of $0.9 \times 0.9 \times 3.0$ mm. The temporal interval between two images of the series is about one week. The data from the BIOMORPH project consist in $256 \times 256 \times 24$ images with a voxel size of $0.9 \times 0.9 \times 5.0$ mm. The temporal interval between two images of the series is about four weeks.

---

[1] Dr Guttman and Dr Kikinis
[2] http://www.cs.unc.edu/~styner/biomorph/biomorph.html

1.2 Quantitative Measurements

A quantitative analysis is required to give accurate and reproducible results, and because the data are large. Between two examinations, a patient does not have the same position in the acquisition device. Therefore images at different times are not directly comparable. We have to apply a transformation to each image to compensate for the difference in position (translation) and orientation (rotation). Then we can compare the two images, and apply automatic computerized tools to detect and quantify evolving processes There are several existing automatic methods to study the lesions of multiple sclerosis in time series:

- With a single image, it is possible to threshold or to study the image intensity to segment lesions [1]. Unfortunately, thresholding does not always make it possible to distinguish the lesions from the white matter.
- It is possible to subtract two successive images to find areas where the lesions have changed. But this method has two major problems. First, the subtraction is extremely dependent on the rigid registration [2], [3]. For instance, we show in Fig. 13 an evolving lesion that appears in the image of the subtraction as a dark hole. But when the registration is inaccurate, it is hard to distinguish evolving lesions: the edges of the anatomical structures appear (cortex, ventricles, etc.) and give the same apparent information as the lesions. Secondly, the subtraction only characterizes the difference of intensity between two images. The image of the subtraction does not give a contrasted image with respect to the evolution ratio, but only with respect to the difference between the intensity of the lesion and the intensity of the background. For example we show in Fig. 1 that if we threshold the image of the subtraction, only some parts of the evolving structures are detected. Moreover the threshold value is not related to the amplitude of the evolutions as can be seen in Fig. 1 where a series of threshold values is applied to a synthesis example.
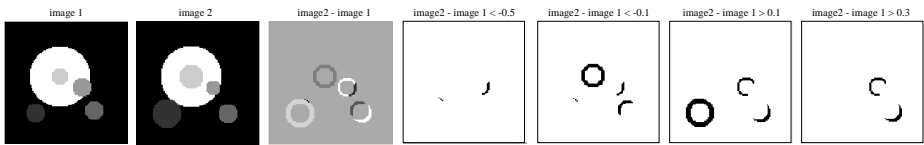

Fig. 1. Different threshold values applied to an image of subtraction. For each value, only some parts of the evolving structures are detected. Moreover, the threshold value is not related to the amplitude of the evolutions

- With n images, it is possible to follow the intensity of each voxel in time [4]. Although very nice results are obtained with perfectly rigidly aligned, the approach remains sensitive to the rigid registration, and there is no direct relation between the amplitude of evolution and the variation of voxels
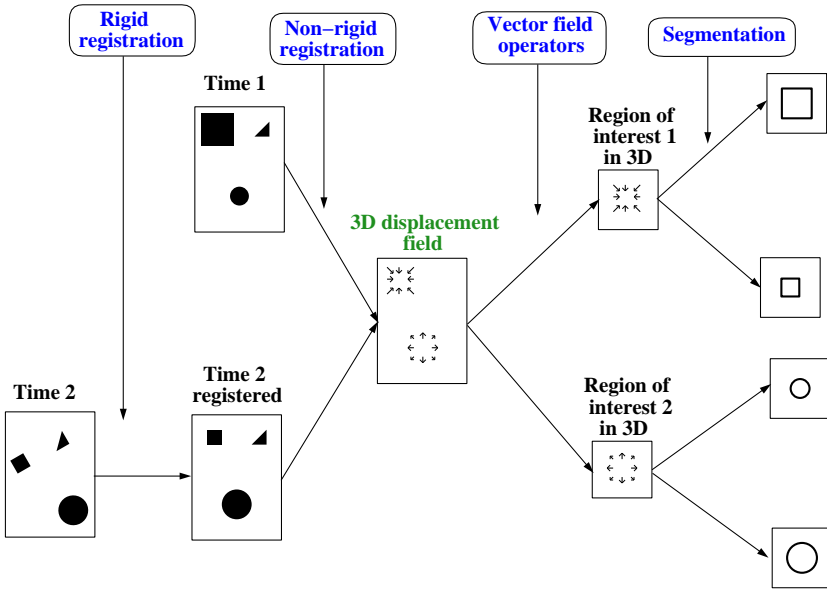
Fig. 2. Method of detection and segmentation of evolving processes using the displacement field

intensity. Moreover, this method does not take into account the spatial correlation between neighboring voxels.

1.3   A New Method Based on the Displacement Field

Our idea is thus to avoid a voxel by voxel comparison and to use the "apparent" motion between two images. Figure 2 shows the different stages of the automatic processing and gives an overview of this paper. First, images are aligned by a rigid registration. Then we compute the displacement field to recover the "apparent" motion between images with a non-rigid registration algorithm. We focus on the detection of the regions of interest of the field thanks to vector field operators, and use them to segment evolving lesions. This work is a natural continuation of the previous research work of Thirion and Calmon [5].

2   Computation of the Displacement Field

2.1   Rigid Registration

First we compute a rigid registration with an algorithm which matches "extremal" points defined as the maxima of the crest lines of the images [6]. Feature points called "extremal" points are automatically extracted from the 3D image. They are defined as the loci of curvature extrema along the "crest lines"
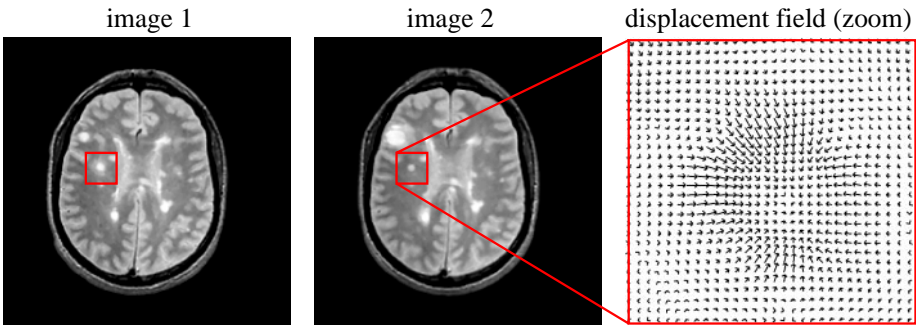
image 1   image 2   displacement field (zoom)

Fig. 3. An example of the computation of the "apparent" displacement field thanks to a non-rigid registration algorithm. Notice how it emphasizes the shrinking lesion

of the isosurface corresponding to the zero-crossing of the Laplacian of the image. Based on those stable points, a two-step registration algorithm computes a rigid transformation. The first step called "prediction" looks for triplets of points from the two sets which can be put into correspondence with respect to their invariant attributes. The second step called "verification" checks whether the 3D rigid transformation computed from the two corresponding triplets is valid for all the other points. A study of the accuracy of this algorithm, especially for aligning MS data, can be found in [7].

2.2 Non-rigid Registration

We compute the 3D displacement field with a non-rigid algorithm based on local diffusion [8]. This algorithm diffuses the first image into the second one. Each point of the second image "attracts" or "repels" the point that has the same coordinates as the first image according to their difference of intensity. All these forces are regularized and deform the second image. The process is iterated based on a multi-scale scheme. At the end, each point $P(x, y, z)^T$ of the reference image has a vector $\mathbf{u}(u_1(P), u_2(P), u_3(P))$ that gives its apparent **displacement** (cf Fig. 3). We can also define the **deformation** which is a function $\Phi(\Phi_1(P), \Phi_2(P), \Phi_3(P))$ that transforms the point $P(x, y, z)^T$ into the point $P'(x', y', z')^T$. We have thus:

$$\begin{cases} x' = x + u_1(x, y, z) = \Phi_1(x, y, z) \\ y' = y + u_2(x, y, z) = \Phi_2(x, y, z) \\ z' = z + u_3(x, y, z) = \Phi_3(x, y, z) \end{cases}$$

This apparent displacement field $\mathbf{u}$ gives an idea of the time evolution between two images. We can compute the two fields: from image 1 to image 2, and from image 2 to image 1, which contain complementary information as we will see in section 4.1. Figure 3 shows the vector field from 1 to 2 around a lesion, emphasizing a radial shrinking. The vector field operators should transform a 3D vector
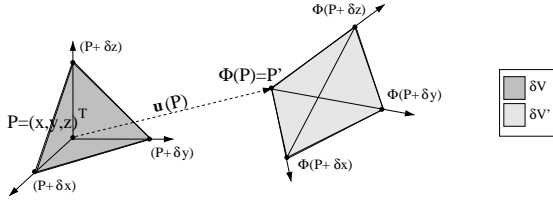
Fig. 4. $\mathbf{u}(P)$ is the apparent displacement of P at time 1. $P' = P+\mathbf{u}(P)$ is the apparent location of P at time 2. The Jacobian of the apparent deformation measures the local volume variation $\frac{\delta V'}{\delta V}$ (see text)

field in a simpler representation that is a 3D scalar image. This scalar image should be contrasted with respect to the time evolutions. Moreover we need to introduce operators that have a physical meaning for a better interpretation.

3   The Jacobian Operator

3.1   Mathematical Expression and Physical Meaning

We introduce as an operator the Jacobian of the deformation function at point P, as suggested from [9]: $\Phi(\Phi_1(P), \Phi_2(P), \Phi_3(P))$. This operator is widely used in continuum mechanics [10] [11]. The Jacobian of Φ at point P is defined as:

$$Jacobian = det(\nabla_p \Phi) = \begin{vmatrix} \frac{\partial \Phi_1}{\partial x} & \frac{\partial \Phi_1}{\partial y} & \frac{\partial \Phi_1}{\partial z} \\ \frac{\partial \Phi_2}{\partial x} & \frac{\partial \Phi_2}{\partial y} & \frac{\partial \Phi_2}{\partial z} \\ \frac{\partial \Phi_3}{\partial x} & \frac{\partial \Phi_3}{\partial y} & \frac{\partial \Phi_3}{\partial z} \end{vmatrix}.$$

It can also be written with the vector displacement field $\mathbf{u}(u_1, u_2, u_3)$ at P:

$$det(\nabla_p \Phi) = det(Id + \nabla_p \mathbf{u}) = \begin{vmatrix} \frac{\partial u_1}{\partial x} + 1 & \frac{\partial u_1}{\partial y} & \frac{\partial u_1}{\partial z} \\ \frac{\partial u_2}{\partial x} & \frac{\partial u_2}{\partial y} + 1 & \frac{\partial u_2}{\partial z} \\ \frac{\partial u_3}{\partial x} & \frac{\partial u_3}{\partial y} & \frac{\partial u_3}{\partial z} + 1 \end{vmatrix}.$$

It is useful to recall a physical interpretation of the Jacobian operator in terms of local variation of volume. With the notations of the Fig. 4, $\mathbf{u}(P)$ is the apparent displacement of P at time 1. $P' = P + \mathbf{u}(P)$ is the apparent location of P at time 2. The volume δV of the elementary tetrahedron defined by $(P, P+\delta x, P+\delta y, P+\delta z)$ is given by:

$$\delta V = \frac{1}{6} \begin{vmatrix} 1 & 1 & 1 & 1 \\ x & x+\delta x & x & x \\ y & y & y+\delta y & y \\ z & z & z & z+\delta z \end{vmatrix} = \frac{1}{6} \begin{vmatrix} 1 & 1 & 1 & 1 \\ 0 & \delta x & 0 & 0 \\ 0 & 0 & \delta y & 0 \\ 0 & 0 & 0 & \delta z \end{vmatrix} = \frac{1}{6}\delta x \delta y \delta z.$$

As we assume that δx is small, a first order approximation of the deformation Φ in P is given by $\Phi(P + \delta x) = \Phi(P) + \frac{\partial \Phi}{\partial x}\delta x + o(\delta x^2)$. We have the same

approximation in y and z directions. Thus the volume $\delta V'$ of the deformed elementary tetrahedron is:

$$\delta V' \simeq \tfrac{1}{6} \begin{vmatrix} 1 & 1 & 1 & 1 \\ 0 & \frac{\partial \Phi_1}{\partial x}\delta x & \frac{\partial \Phi_1}{\partial y}\delta y & \frac{\partial \Phi_1}{\partial z}\delta z \\ 0 & \frac{\partial \Phi_2}{\partial x}\delta x & \frac{\partial \Phi_2}{\partial y}\delta y & \frac{\partial \Phi_2}{\partial z}\delta z \\ 0 & \frac{\partial \Phi_3}{\partial x}\delta x & \frac{\partial \Phi_3}{\partial y}\delta y & \frac{\partial \Phi_3}{\partial z}\delta z \end{vmatrix} = \tfrac{1}{6} Jac_p(\Phi)\delta x \delta y \delta z.$$

Therefore:

$$\delta V' \simeq Jac_p\left(\Phi\right) \cdot \delta V.$$

Thus, the local variation $\frac{\delta V'}{\delta V}$ of an elementary volume is given (as a first order approximation) by the Jacobian of the deformation function Φ. When $Jac_p(\Phi) > 1$ there is a local expansion at point P, and when $Jac_p\left(\Phi\right) < 1$ there is a local shrinking at point P. The transformation is locally preserving the volume when $Jac_p\left(\Phi\right) = 1$.

3.2   Robustness of the Jacobian with Respect to Misalignment

Figure 5 shows what happens when two images are not perfectly aligned: the deformation function Ψ, which is measured, is different from the ideal one Φ. The misregistration is given by a residual rotation R and translation t. We have $\Psi = R \circ \Phi + t$.
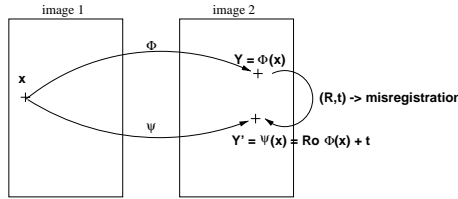

Fig. 5. Φ is the deformation function for a perfect rigid registration, and Ψ is the deformation function when there is a misregistration (R,t). We have $\Psi = R \circ \Phi + t$

Then we have:

$$Jac\left(\Psi\right) = det(\nabla \Psi) = det(\nabla(R \circ \Phi + t)) = det(R \cdot \nabla \Phi) = Jac\left(\Phi\right).$$

Therefore the Jacobian of the theoretical deformation function (for a perfect rigid registration) is equal to the Jacobian of a measured deformation function (whatever the misregistration). Of course this requires that, even in the case of an approximate alignment of images, the non-rigid registration still computes a correct displacement field. In our case the rigid registration is performed because our non-rigid registration algorithm requires a proper initial alignment to give a good result. Nevertheless, the rigid registration does not have to be as accurate as for the subtraction method where a precision better than or equal to one voxel is required.

3.3   Computation and Application of the Jacobian

We have seen that the computation of the Jacobian of the deformation Φ can be performed directly with the displacement field **u**. We need to compute the first 9 derivatives of the displacement field **u**: $\frac{\partial u_x}{\partial x}, \frac{\partial u_x}{\partial y}, \frac{\partial u_x}{\partial z}, \ldots, \frac{\partial u_z}{\partial z}$. For a faster computation we use recursive filtering that gives an image for each derivative. Then, we need to store in memory the 9 derivatives to compute the Jacobian and for an image of $256 \times 256 \times 180$ this requires about 425M-bytes of memory. So to avoid overfilling the memory space we compute the Jacobian on sub-images and then we fuse the different sub-results which include an overlapping border to avoid side effects.

The Jacobian gives a contrasted image with respect to the evolution amplitude. The most contrasted areas tend to correspond to shrinking or growing lesions. In Fig. 6 we see that an important shrinking of a lesion between two images gives a dark region in the Jacobian image. On other areas, the value is almost constant and very close to 1, which indicates no apparent variation of volume. A zoom around a lesion shows that darker areas correspond to shrinking lesions.
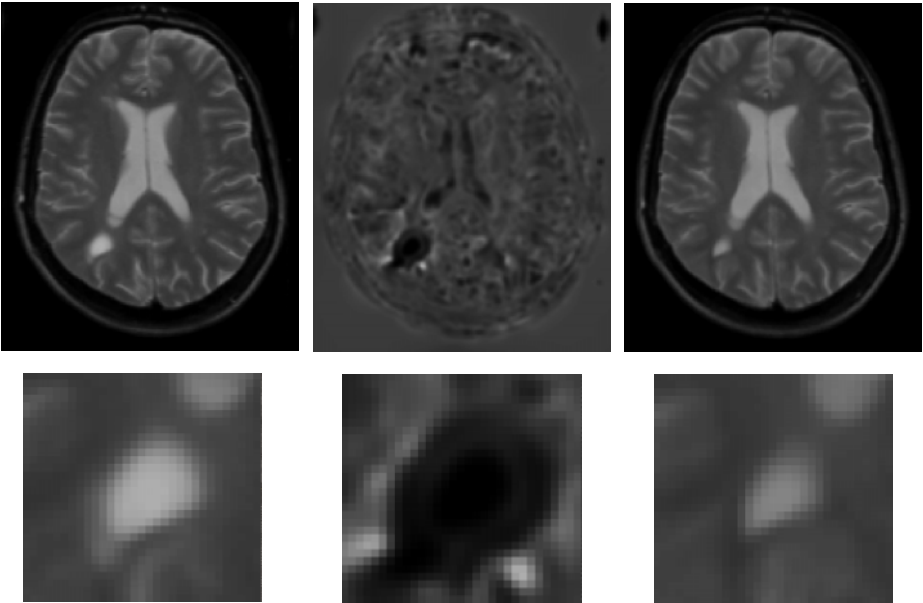

Fig. 6. Application of the Jacobian: we can see a lesion that shrinks

3.4   Other Operators

Calmon and Thirion have developed another vector field operator based on the divergence and the norm of the displacement field $\mathbf{u}$ [12] [13]:

$$norm \cdot div(P) = \|\mathbf{u}(P)\| div\ \mathbf{u}(P) = \|\mathbf{u}(P)\|(\frac{\partial u_1}{\partial x} + \frac{\partial u_2}{\partial y} + \frac{\partial u_3}{\partial z}).$$

This operator has no simple physical meaning even if the sign of the operator gives information about shrinking (negative values) or expansion (positive values). As we have no physical interpretation of the value, it is difficult to threshold the image automatically in order to extract the regions of interest.

Prima et al. proposed another operator which gives the local variation of volume [14]. A cell of voxels of volume is V_1 is deformed to a complex polyhedron which volume V_2 is computed. Then $\frac{V2-V1}{V1}$ is calculated. Note that another algorithm to compute V_2 is given in [15]. This operator is directly related to the Jacobian:

$$\frac{V_2 - V_1}{V_1} = \frac{V_2}{V_1} - 1 \simeq Jac - 1.$$

Figure 7 shows the application of these three operators on the same displacement field. In particular we can notice how the Jacobian and the discrete computation of the relative variation of volume are similar. The advantage of our approach is that it provides a continuous framework for a computation of the Jacobian at any scale.
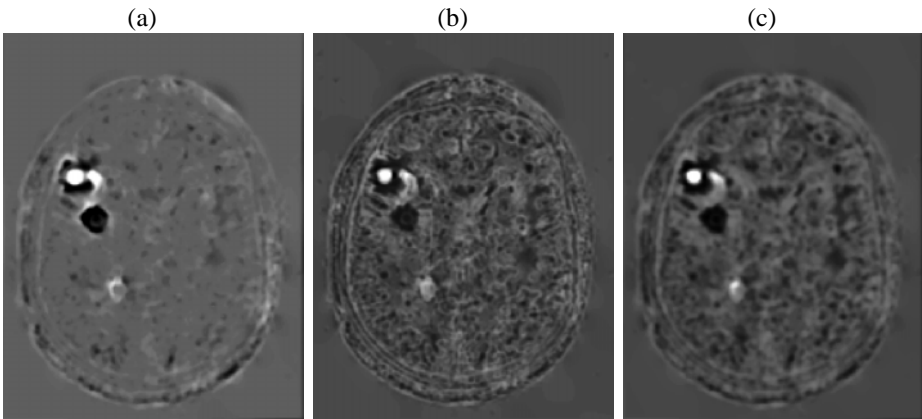
(a)   (b)   (c)

Fig. 7. Comparison between different existing operators. (a): $\|\mathbf{u}\| div\ \mathbf{u}$. (b): discrete computation of $\frac{V_2-V_1}{V_1} \sim (Jac\ (\Phi) - 1)$. (c): Jacobian

4   Results

4.1   Thresholding and Segmentation

We can extract the areas that correspond to a significant time evolution. It is possible to find a uniform threshold over the whole Jacobian image relying on its physical interpretation in terms of local variation of volume. We chose an empiric threshold of 0.3 for significant shrinking. An example in Fig. 8 shows that it gives a good segmentation of a shrinking lesion. correspond to shrinking lesions. In
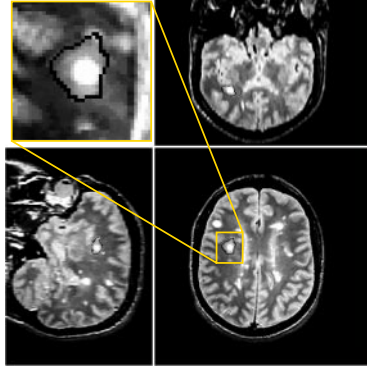

Fig. 8. The threshold $det(\nabla\Phi) < 0.3$ makes it possible to segment shrinking lesions

fact, we are going to focus only on the shrinking areas. We can see in Fig. 9 that a better description is provided with the shrinking field. If there is an important expansion locally between images 1 and 2, we would need a one to many mapping due to limited resolution of the image. To avoid this, we consider only shrinking regions from 1 to 2, and then shrinking regions from 2 to 1. By thresholding shrinking areas we obtain the segmentations $s_{1\rightarrow2}$ in the first image, and $s_{2\rightarrow1}$ in the second image. Then we have to combine those two information: the whole segmentations in image 1 and 2 are given by $S_{12}(t1) = [s_{1\rightarrow2}] \cup [\mathbf{u}_{2\rightarrow1}(s_{2\rightarrow1})]$, and $S_{12}(t2) = [s_{2\rightarrow1}] \cup [\mathbf{u}_{1\rightarrow2}(s_{1\rightarrow2})]$. Figures 10 show automatic segmentation results obtained at two times.

With the fields between images 1 and 2 and between images 2 and 3, we can compute segmentations S_{12} in the images 1 and 2 and S_{23} in the images 2 and 3. Then we propagate the segmentations S_{12} and S_{23} respectively to times $t3$ and $t1$, thanks to the vector fields $\mathbf{u}_{21}$ and $\mathbf{u}_{23}$. Then by addition, we obtain a segmentation of the lesions in all the images of a series ([16]). In Fig. 11, we can see the result of this method on three successive instances.

4.2   Study on a Synthetic Example

We have created two images I_1 and I_2, by including two artificial evolving 3-D lesions into the same 3-D T2 weighted image of a brain without lesions. The

field from 1 to 2 (expansion)   field from 2 to 1 (shrinking)

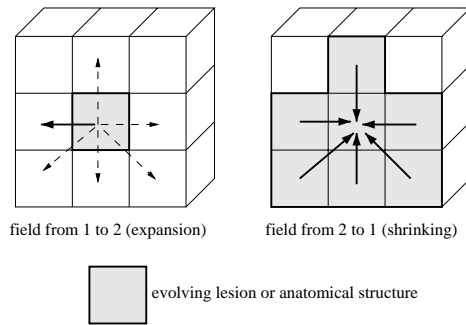evolving lesion or anatomical structure

Fig. 9. The information is richer when we look at the shrinking field. Left: If there is a large expansion, the direct displacement field cannot express that one voxel should deform to several voxels. We would need a one to many mapping due to limited resolution of the image. Right: Thanks to the reverse field, a better description of the phenomenon is possible
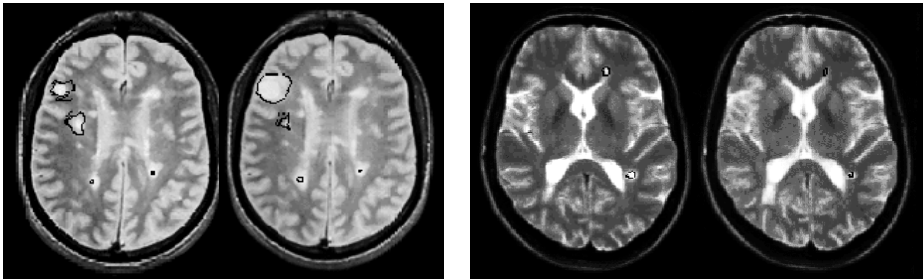

Fig. 10. Segmentation of evolving lesions. Left: Brigham & Women's Hospital data. Right: BIOMORPH data

artificial lesions are represented by spheres of radius respectively 10mm and 4mm in I_1, and 6mm and 8mm in I_2 (Fig. 12a). Because the global rigid registration of I_1 and I_2 is the identity in this case, we have only applied the non-rigid registration algorithm to compute the direct and reverse local displacement field everywhere. We have then applied our method to extract the boundary of evolving regions, with $Jac(\Phi) < 0.3$. Results on Fig. 12c show that the evolving regions are correctly detected. The accuracy of the delimitation of the boundary is qualitatively correct, but we observed a difference between 5 and 20 percent between the correct diameter of lesions and the measured one.

4.3   Robustness with Respect to Imperfect Rigid Registration

From the previous example, we also created an image I_2' by translating I_2 by 3 voxels in one direction. As expected, our method provides similar results when
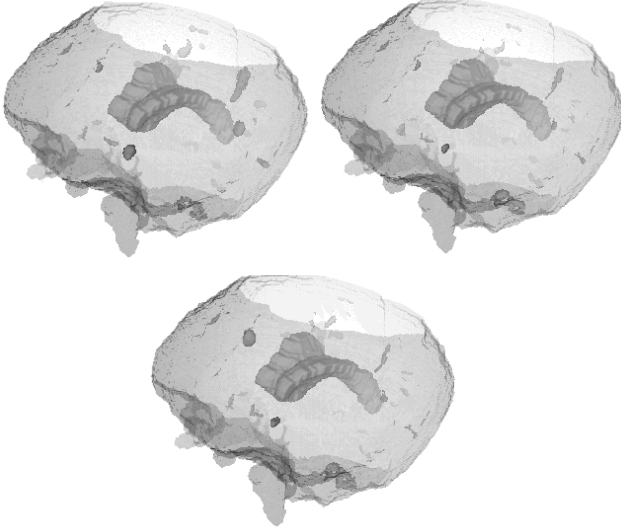
Fig. 11. Thanks to the segmentation of the evolutions between times 1 and 2, and between times 2 and 3, it is possible to visualize the lesions evolution between the 3 successive acquisitions

applied to I_1 and I'_2 (Fig. 12e) , while a simple difference yields very noisy results (Fig. 12d).

We also considered the application of our method between two real T2 weighted MR image, Im_1 and Im_2 (same 3D images as the ones presented in Fig. 3). When Im_1 and Im_2 are perfectly rigidly registered, our method produces the segmentation of an evolving lesion in the cross-section shown in Fig. 13b, which can be compared to a simple difference analysis between the registered images (Fig. 13a). We also created an image Im'_2 by adding a misalignment to I_2 corresponding to a rotation of 1 degree around an axis orthogonal to this cross-section and passing through its center, plus a translation of 1 voxel in the two directions of the plane of this cross-section. We observe that the results provided by our method (Fig. 13c) remain similar to the results of Fig. 13b, whereas a simple difference now produces very noisy results (Fig. 13d).

5   Conclusion

In this article we proposed a new method to study multiple sclerosis lesions evolution through time based on the apparent displacement field between images. We believe that our approach will be useful to detect evolving regions corresponding to local apparent expansion or shrinking. As this method is robust with respect to imperfect rigid alignment, we plan to use it in combination with
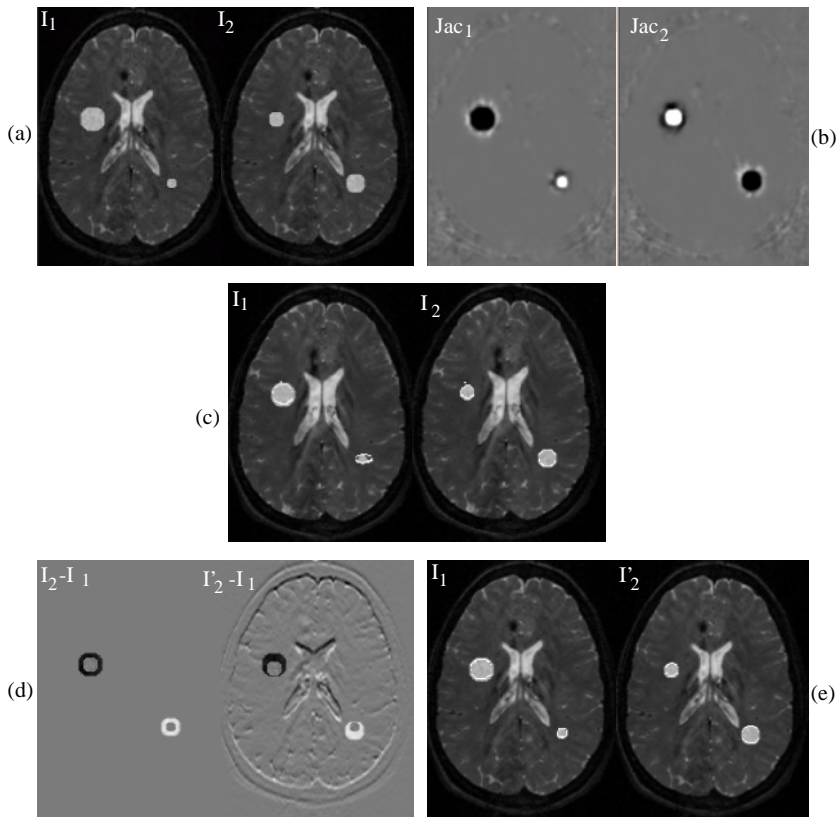
Fig. 12. (a): two synthetic temporal images I_1 and I_2. (b): the Jacobian image of the field from I_1 to I_2 and I_2 to I_1. (c): automatic segmentation of evolving lesions in I_1 and I_2 using $Jac(\Phi) < 0.3$. (d): $I_2 - I_1$ on the left. On the right $I_2' - I_1$ where I_2' is a translated version of I_2. (e): automatic segmentation of evolving lesions in I_1 and I_2', which shows robustness to imperfect rigid registration of images

other segmentation algorithms in order to delineate more precisely the boundary of the lesions in temporal sequences. Then we will compare our results with manual and other automatic segmentation results [17]. This will be done within the BIOMORPH project. Finally we plan to apply our approach to study the "mass effect" by quantifying the evolution of anatomical structures such as the cerebral ventricles or the interface between grey matter and white matter.
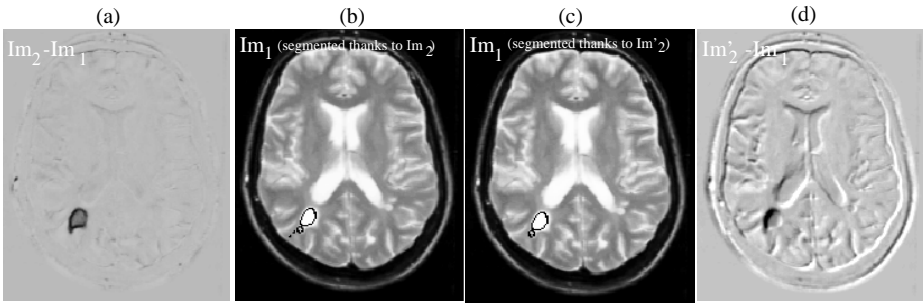
Acknowledgments

Fig. 13. Segmentation of evolving lesions in Im_1 thanks to the study between Im_1 and Im_2 (perfectly rigidly registered) and between Im_1 and Im_2' where Im_2' is a misregistered version of Im_2. This study shows the robustness with respect to imperfect rigid registration. (a): $Im_2 - Im_1$. (b): automatic segmentation in Im_1 thanks to the study between Im_1 and Im_2. (c): automatic segmentation in Im_1 thanks to the study between Im_1 and Im_2'. (d): $Im'2 - Im_1$

References

1. Zijdenbos, A. and Forghani, R. and Evans, A.: Automatic Quantification of MS Lesions in 3D MRI Brain Data Sets: Validation of INSECT. In: Wells, W.M. and Colchester, A. and Delp, S. editors, the First International Conference on Medical Image Computing and Computer-Assisted Intervention MICCAI'98, volume 1496 of Lecture Notes in Computer Science, 439-448, Boston (1998).
2. Hajnal, J.V. and Saeed, N. and Oatridge, A. and Williams, E.J. and Young, I.R. and Bydder, G.: Detection of Subtle Brain Changes Using Subvoxel Registration and Substraction of Serial MR Images. Journal of Computer Assisted Tomography, **5** (1995) 677-691
3. Lemieux, L.: The Segmentation and Estimation of Noise in Difference Images of Co-registered MRI Scan Pairs. In: Medical Image Understanding and Analysis (MIUA'97), Oxford (1997). Electronic version : http://www.robots.ox.ac.uk/˜mvl/frame_proceedings.html#Registration
4. Gerig, G. and Welti, D. and Guttman, C. and Colchester, A. and Székely, G.: Exploring the Discrimination Power of the Time Domain for Segmentation and Characterization of Lesions in Serial MR Data. In: Wells, W.M and Colchester, A. and Delp, S. editors, the First International Conference on Medical Image Computing and Computer-Assisted Intervention, MICCAI'98, volume 1496 of Lecture Notes in Computer Science, 469-480, Boston (1998)

5. Thirion, J.P. and Calmon, G.: Measuring Lesion Growth from 3D Medical Images. In: IEEE Nonrigid and Articulated Motion Workshop (NAN'97), Puerto Rico (1997). Electronic version: http://www.inria.fr/RRRT/RR-3101.html

6. Thirion, J.P.: New Feature Points Based on Geometric Invariants for 3D Image Registration. International Journal of Computer Vision, **2** (1996) 121-137. Electronic version: http://www.inria.fr/RRRT/RR-1901.html

7. Pennec, X. and Thirion, J.P.: A Framework for Uncertainty and Validation of 3D Registration Methods based on Points and Frames. IJCV, **3** (1997) 203-229. Electronic version: http://www.inria.fr/epidaure/personnel/pennec/Publications.html

8. Thirion, J.P.: Image matching as a diffusion process: an analogy with Maxwell's demons. Medical Image Analysis, **2** (1998) 243-260. Electronic version: http://www.inria.fr/RRRT/RR-2547.html

9. Davatzikos, C. and Vaillant, M. and Resnick, S. and Prince, J.L. and Letovsky, S. and Bryan, R.N.: Morphological Analysis of Brain Structures Using Spatial Normalization. In: Höhne, K.H. and Kikinis, R. editors, Visualization in Biomedical Computing, volume 1131 in Lecture Notes in Computer Science, 355-360, Hamburg (1996). Electronic version : http://iacl.ece.jhu.edu/~prince/jlp_pubs.html.

10. Bro-Nielsen, M.: Medical Image Registration and Surgery Simulation. PhD thesis, IMM, (1997)
Electronic version: http://www.imm.dtu.dk/documents/users/bro/phd.html.

11. Weiss, J.A. and Maker, B.N. and Govindjee, S.: Finite Element Implementation of Incompressible, Transversely Isotropic Hyperelasticity. Computer Methods in Applied Mechanics and Engineering, number 135 (1997) 107-128

12. Thirion J.P. and Calmon, G.: Deformation Analysis to Detect and Quantify Active Lesions in 3D Medical Image Sequences. Research Report 3101, INRIA (1997). Electronic version: http://www.inria.fr/RRRT/RR-3101.html

13. Thirion, J.P. and Prima, S. and Subsol, G.: Statistical Analysis of Dissymmetry in Volumetric Medical Images. Research Report 3178, INRIA (1997). Electronic version: http://www.inria.fr/RRRT/RR-3178.html

14. Prima, S. and Thirion, J.P. and Subsol, G. and Roberts, N.: Automatic Analysis of Normal Brain Dissymmetry of Males and Females in MR Images. In: Wells, W.M. and Colchester, A. and Delp, S. editors, the First International Conference on Medical Image Computing and Computer-Assisted Intervention, MICCAI'98, volume 1496 of Lecture Notes in Computer Science, 770-779, Boston (1998)

15. Calmon, G. and Roberts, N. and Eldridge, P. and Thirion, J.P.: Automatic Quantification of Changes in the Volume of Brain Structures. In: Wells, W.M. and Colchester, A. and Delp, S. editors, the First International Conference on Medical Image Computing and Computer-Assisted Intervention, MICCAI'98, volume 1496 of Lecture Notes in Computer Science, 964-973, Boston (1998)

16. Rey, D and Subsol, G. and Delingette, H. and Ayache, N.: Automatic detection and segmentation of evolving processes in 3D medical images: application to multiple sclerosis. Research Report 3559, INRIA (1998). Electronic version: http://www.inria.fr/RRRT/RR-3559.html

17. Bello, F. and Colchester, A.: Measuring Global and Local Spatial Correspondence Using Information Theory. In: Wells, W.M. and Colchester, A. and Delp, S. editors, the First International Conference on Medical Image Computing and Computer-Assisted Intervention, MICCAI'98, volume 1496 of Lecture Notes in Computer Science, 964-973, Boston (1998)